A Structure-Based Mechanism for Copper−Zinc Superoxide Dismutase[†,‡]

P. John Hart,[§,||,⊥] Melinda M. Balbirnie,[||] Nancy L. Ogihara,[||] Aram M. Nersissian,[||] Manfred S. Weiss,[§,||,#] Joan Selverstone Valentine,*[,||] and David Eisenberg*[,§,||,Δ]

UCLA-DOE Laboratory of Structural Biology and Molecular Medicine and Departments of Chemistry and Biochemistry and Biological Chemistry, University of California, Los Angeles, California 90095

Received September 22, 1998; Revised Manuscript Received December 11, 1998

ABSTRACT: A reaction cycle is proposed for the mechanism of copper−zinc superoxide dismutase (CuZnSOD) that involves inner sphere electron transfer from superoxide to Cu(II) in one portion of the cycle and outer sphere electron transfer from Cu(I) to superoxide in the other portion of the cycle. This mechanism is based on three yeast CuZnSOD structures determined by X-ray crystallography together with many other observations. The new structures reported here are (1) wild type under 15 atm of oxygen pressure, (2) wild type in the presence of azide, and (3) the His48Cys mutant. Final *R*-values for the three structures are respectively 20.0%, 17.3%, and 20.9%. Comparison of these three new structures to the wild-type yeast Cu(I)ZnSOD model, which has a broken imidazolate bridge, reveals the following: (i) The protein backbones (the "SOD rack") remain essentially unchanged. (ii) A pressure of 15 atm of oxygen causes a displacement of the copper ion 0.37 Å from its Cu(I) position in the trigonal plane formed by His46, His48, and His120. The displacement is perpendicular to this plane and toward the NE2 atom of His63 and is accompanied by elongated copper electron density in the direction of the displacement suggestive of two copper positions in the crystal. The copper geometry remains three coordinate, but the His48−Cu bond distance increases by 0.18 Å. (iii) Azide binding also causes a displacement of the copper toward His63 such that it moves 1.28 Å from the wild-type Cu(I) position, but unlike the effect of 15 atm of oxygen, there is no two-state character. The geometry becomes five-coordinate square pyramidal, and the His63 imidazolate bridge re-forms. The His48−Cu distance increases by 0.70 Å, suggesting that His48 becomes an axial ligand. (iv) The His63 imidazole ring tilts upon 15 atm of oxygen treatment and azide binding. Its NE2 atom moves toward the trigonal plane by 0.28 and 0.66 Å, respectively, in these structures. (v) The replacement of His48 by Cys, which does not bind copper, results in a five-coordinate square pyramidal, bridge-intact copper geometry with a novel chloride ligand. Combining results from these and other CuZnSOD crystal structures, we offer the outlines of a structure-based cyclic mechanism.

Higher organisms produce superoxide anion (O_2^-) as an occasional byproduct during the one-electron reduction of dioxygen that occurs in respiration and photosynthesis (*1*, *2*). Also, in animals, macrophages generate superoxide as part of the immune response (*3*, *4*). Organisms must therefore have ways to regulate superoxide concentrations since excess amounts can inactivate enzymes containing iron−sulfur clusters and can lead to the formation of highly oxidizing species (such as hydroxyl radical) damaging to other cellular constituents (*5*).

Copper−zinc superoxide dismutase (CuZnSOD)[1] is a 32 kDa homodimeric protein in the cytoplasm of eucaryotic and bacterial cells that catalyzes the disproportionation of superoxide into dioxygen and hydrogen peroxide ($2O_2^- + 2H^+ \rightarrow O_2 + H_2O_2$) (*6*, *7*). Each monomer of the molecule binds one copper and one zinc ion and displays the Greek Key β-barrel fold (*8*). The enzymatic mechanism proposed for CuZnSOD is reduction of the oxidized Cu(II) form of the enzyme by superoxide, releasing dioxygen (reaction 1), alternating with oxidation of the reduced Cu(I) form by

[†] This research was supported by grants from the Amyotrophic Lateral Sclerosis Association (ALSA) (award 012591 to D.E.), the NIH (GM31299 to D.E. and GM28222 to J.S.V.), and the DOE (DE-FC03-87ER60615), in part by an appointment (to P.J.H.) to the Alexander Hollaender Distinguished Postdoctoral Fellowship Program, sponsored by the U.S. Department of Energy, Office of Health and Environmental Research, and administered by the Oak Ridge Institute for Science and Education, and in part by the National Institutes of Health Chemistry/Biology Interface Predoctoral Training at UCLA (M.M.B. and N.L.O.).

[‡] The coordinates have been deposited in the Brookhaven Protein Data Bank (file names 2jcw, 1b4l, 1yaz, and 1b4t).

[§] UCLA-DOE Laboratory of Structural Biology and Molecular Medicine.

[||] Department of Chemistry and Biochemistry, UCLA.

[⊥] Present address: Department of Biochemistry, The University of Texas Health Science Center at San Antonio, 7703 Floyd Curl Drive, San Antonio, TX 78284-7760.

[#] Present address: Institute of Molecular Biotechnology, Department of Structural Biology and Crystallography, Beutenbergstrasse 11, D-07745 Jena, Germany.

[Δ] Department of Biological Chemistry, UCLA.

[1] Abbreviations: CuZnSOD, copper−zinc superoxide dismutase; yWT, wild-type yeast CuZnSOD; yAB, azide-bound yeast CuZnSOD; bAB, azide-bound bovine CuZnSOD; H48C, histidine 48 to cysteine (copper ligand mutant) yeast CuZnSOD; 15 atm, 15 atmospheres of oxygen pressure yeast CuZnSOD; Xeno, *Xenopus laevis* CuZnSOD; bRED, reduced bovine CuZnSOD; G37R, human Gly37 to Arg FALS mutant CuZnSOD; FALS, familial amyotrophic lateral sclerosis; rms, root mean square; AU, asymmetric unit.

10.1021/bi982284u CCC: $18.00
Published on Web 01/29/1999

Table 1: States of Eucaryotic CuZnSOD Observed by X-ray Crystallography

species	ligands	Cu bridge	Cu geometry	PDB code	AU	ref
bovine	4 His, 1 H_2O	intact	square planar	2SOD	2 dimers	*8*
bovine Cu(II)/Co	4 His, 1 H_2O	intact	square planar	1COB	1 dimer	*53*
bovine Cu(I)/Co	4 His, 1 H_2O	intact	square planar	2SXC	1 dimer	*29*
bovine $^-N_3$-bound	4 His, 1 $^-N_3$	intact	square pyramidal	1SXZ	1 dimer	*49, 56*
bovine thiocyanate	4 His, 1 $^-$SCN	intact	square planar	1SXS	1 dimer	*56*
bovine C6A	4 His, 1 H_2O	intact	square planar	3SOD	2 dimers	*65*
Xenopus	4 His, 1 H_2O	intact	square planar	1XSO	1 dimer	*48*
Xenopus CN-bound	4 His, 1 CN	intact	square planar	1XSO	1 dimer	*21*
spinach	4 His, 1 H_2O	intact	square planar	1SRD	2 dimers	*18*
human	4 His	intact	square planar	1SPD	1 dimer	*64*
human	4 His	intact	square planar	1SOS	5 dimers	*20*
human FALS mutant	4 His, 1 subunit	intact	square planar	1AZV	1 dimer	*50*
G37R	3 His, 1 subunit	broken	trigonal planar			
yeast	4 His, 1 H_2O	intact	square planar	1SDY	2 dimers	*19*
yeast Cu(I)	3 His	broken	trigonal planar	1JCW	1 monomer	*26*
yeast, 15 atm of oxygen	3 His	broken	trigonal planar	1b4l	1 monomer	this study
yeast $^-N_3$-bound	4 His, 1 $^-N_3$	intact	square pyramidal	1yaz	1 monomer	this study
yeast H48C	3 His, 1 Cl^-, 1 H_2O	intact	square pyramidal	1b4t	1 monomer	this study

another superoxide anion and two protons, generating hydrogen peroxide (reaction 2) (*9*−*12*).

$$O_2^- + \text{Cu(II)ZnSOD} \rightarrow O_2 + \text{Cu(I)ZnSOD} \quad (1)$$

$$O_2^- + \text{Cu(I)ZnSOD} + 2H^+ \rightarrow H_2O_2 + \text{Cu(II)ZnSOD} \quad (2)$$

Crystallographic and spectroscopic studies demonstrate that a histidyl residue (His63 in human and yeast) coordinates the copper and zinc ions simultaneously in the cupric form of the enzyme. This histidine residue, termed the "histidine bridge" or "bridging imidazolate", is a motif so far observed only in CuZnSOD. In the cupric form of SOD the copper binding geometry is described as distorted square planar, with histidine residues 46, 48, 63, and 120 acting as ligands in the human and yeast proteins (*8, 13*−*21*). A water molecule is found approximately 2.5 Å from the Cu(II) ion, weakly coordinating in an axial position relative to the distorted square plane formed by the histidine ligands (*8, 14, 19, 20, 22*−*25*).

In the cuprous form of the enzyme, several crystallographic and spectroscopic analyses indicate that the bridging imidazolate is lost as a copper ligand because of protonation of the NE2 atom of the bridging histidine on the copper binding side.

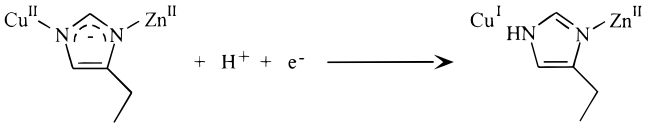

In these studies, the loss of the His63−Cu bond upon copper reduction results in a nearly trigonal planar copper coordination geometry with histidine residues 46, 48, and 120 acting as ligands (*15, 22, 26*−*28*). Yet a crystallographic determination of the Cu(I) form of the bovine enzyme revealed an intact imidazolate bridge (*29*). Nevertheless, most of the data from solution studies suggest strongly that the imidazolate bridge that is present in the Cu(II) form of the enzyme breaks and re-forms during superoxide dismutase catalysis. Table 1 summarizes the active site states observed crystallographically in CuZnSOD.

In both steps of the disproportionation reaction mechanism, superoxide is guided to the active site channel by a conserved set of charged amino acid residues (*30*−*32*). The channel containing these charges narrows from a shallow depression about 24 Å across to a deeper channel about 10 Å wide and finally to an opening of less than 4 Å just above the copper ion. The guanidinium group of Arg143 is located approximately 5.8 Å from the copper, where it attracts negatively charged species to the channel entrance and, with Thr137, sterically excludes large nonsubstrate anions (*33*). Some small anions such as cyanide, azide, and fluoride, however, do enter the active site cavity and competitively inhibit the enzyme, presumably by binding directly to the copper ion (*34, 35*). Nuclear magnetic resonance studies indicate that some anions such as chloride and phosphate can enter the channel but do not bind directly to the copper. They instead remain associated with Arg143 in the active site channel in an "anion binding site" about 5.5 Å away from the copper ion (*36, 37*).

To learn more about the mechanism of action of SOD, we determined three additional yeast CuZnSOD structures: 15 atm of oxygen, azide-bound, and the H48C mutant. We assume these structures provide information on states in the mechanistic pathway of SOD action. The questions that arise from comparison of these structures and those in Table 1 include the following: (1) Can protein−protein interactions in the crystal modulate redox potentials of bound metals? (2) Are protein backbone changes involved in the mechanism? (3) Does superoxide bind to copper or does it transfer its electron indirectly? (4) What are the structural roles of the histidine copper ligands, Arg143, and conserved active site water molecules in the mechanism? (5) Which protons transfer to superoxide as it is reduced to hydrogen peroxide?

As a reference for these ligand and mutant studies, we use the crystal structure of yeast CuZnSOD refined to 1.7 Å (20 °C) and 1.55 Å (−180 °C) resolution (*26*). The molecules pack in the crystal structure with the CuZnSOD molecular 2-fold axis coincident with a crystallographic 2-fold axis. That is, the yeast wild-type CuZnSOD exhibits exact 2-fold molecular symmetry. The structure also demonstrates an unexpected feature in that, unlike all previously determined CuZnSOD structures (including those with the copper ion forcefully reduced using exogenous reductants), the imid-

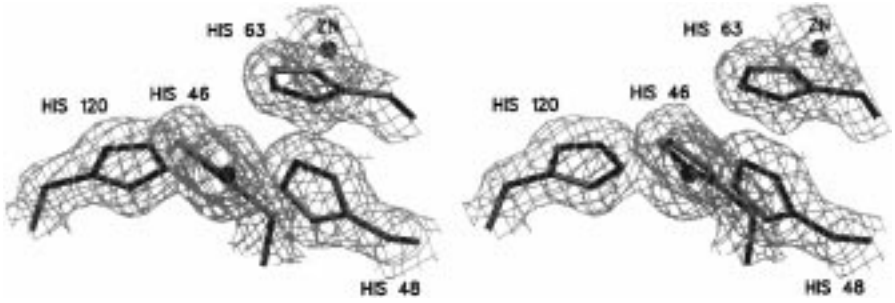

FIGURE 1: Atomic model for the active site atoms of yeast wild-type CuZnSOD superimposed on 1.7 Å resolution electron density of the form $(2F_o - F_c)\alpha_c$ contoured at 1σ (*26*). The copper ion is 3.16 Å from the NE2 atom of the bridging imidazolate, His63. It is held by a trigonal planar arrangement of histidine residues (His46, His48, and His120). Notice that the imidazolate bridge to the copper ion is broken.

azolate bridge is broken and the copper ion is coordinated by a roughly trigonal planar ligand geometry (His46, His48, His120) characteristic of the Cu(I) rather than the Cu(II) oxidation state (Figure 1). This occurs even though the crystals are grown in air and without reducing agent present. EPR spectroscopy on the crystals confirms that the copper ion is reduced (*26*).

Comparison of these three new yeast CuZnSOD structures with previous SOD structures offers the beginnings of a structure-based catalytic cycle for SOD.

MATERIALS AND METHODS

Protein and Crystals. Wild-type CuZnSOD from *Saccharomyces cerevisiae* (yeast wild type) was purchased from Carlbiotech Ltd., Copenhagen. The H48C mutant yeast CuZnSOD molecule was prepared by site-directed mutagenesis on template DNA encoding wild-type yeast SOD according to procedures previously described (*38, 39*). The H48C mutant gene was subcloned into a pET-3d plasmid (Stratagene) and expressed in *Escherichia coli* strain BL21(DE3) under the control of the IPTG-inducible lac UV5 promoter. The protein was purified via anion-exchange chromatography on DEAE-cellulose (Whatman) followed by gel filtration on Sephadex G-75 (Pharmacia). The identity and purity of the H48C CuZnSOD mutant, which gives a single band on a 15% SDS−PAGE, were confirmed by electrospray ionization mass spectrometry.

To remove adventitiously bound metals, purified H48C was subjected to dialysis against 100 mM acetate buffer, pH 3.8, and 100 mM EDTA, followed by dialysis with the same buffer but with 100 mM NaCl replacing the EDTA, followed by dialysis against 100 mM acetate, pH 5.5. The H48C apoprotein concentration was calculated using a molar extinction coefficient of 3000 M^{-1} cm^{-1} at 278 nm (derived from the single tyrosine residue per protein monomer). H48C was remetalated with zinc first, followed by copper as described previously (*40*). The reconstituted protein was finally dialyzed against 50 mM phosphate, pH 7.7, and concentrated to ∼150 mg/mL using a Centricon 10 spin concentrator (Amicon).

Lyophilized wild-type yeast CuZnSOD was dissolved to 15−25 mg/mL, also in 50 mM phosphate buffer (pH 7.7). Both protein solutions were mixed with an equal volume (5 μL) of reservoir solution containing 2.0−2.2 M ammonium sulfate, 50 mM Tris-HCl, pH 7.5, 50 mM NaCl, and 0.001% (w/v) NaN_3 and allowed to equilibrate at room temperature (wild type) and 4 °C (H48C). Large rhomboid crystals grew within 2 weeks in space group *R*32 (*26*).

Partially oxidized yeast CuZnSOD crystals were prepared by exposing wild-type *R*32 crystals [Cu(I)] to ∼15 atm of O_2 using a specially designed goniometer head (*41*). The design allows the researcher to evacuate and then pressurize a capillary containing the crystal with any gas of interest. The gas pressure can be maintained over the entire course of the data collection experiment. The crystals, which are colorless when grown at 1 atm, appeared light blue after 1 h of oxygen treatment. The crystals were maintained at ∼15 atm of oxygen pressure for the duration of the X-ray experiment.

Azide-bound crystals were prepared by transferring a suitable yeast wild-type crystal into a 10 μL drop of artificial mother liquor [50 mM Tris-HCl, pH 7.5, 50 mM NaCl, 2.3 M ammonium sulfate, 0.001% (w/v) NaN_3] placed on a 13 mm, 0.025 μm pore size filter disk (Filter Type VS, Millipore). The filter disk was then floated on 1.0 mL of artificial mother liquor made 500 mM in NaN_3 in a Linbro plate reservoir. The well was sealed with a cover slip. Azide diffuses into the drop as low molecular weight species exchange across the membrane (*42*). After 1 week, crystals were harvested for X-ray data collection. The crystals appeared pale green due to the azide nitrogen-to-copper charge-transfer band at ∼375 nm. Azide-bound crystals were also produced via cocrystallization by addition of NaN_3 in concentrations ranging from 0.25 to 1.0 M to the yeast wild-type crystallization protocol. Crystals formed by this method were not used for X-ray data collection, however, because nucleation events were much more numerous, leading to significantly smaller azide-bound crystals.

Diffraction Data. High-resolution diffraction data were taken from different X-ray sources. The 15 atm of oxygen diffraction data were collected using synchrotron radiation from SSRL beamline 7-1. Azide-bound and H48C crystal data were collected on a Rigaku RU-200 rotating anode X-ray generator. All data were recorded on imaging plate detectors (MAR for synchrotron data and RAXIS IV for rotating anode data). Table 2 summarizes parameters and statistics of data collection on the three types of crystals.

Refinement. Wild-type, 15 atm of oxygen, azide-bound, and H48C crystals were isomorphous in space group *R*32. For each of the three new crystals, the wild-type structure of yeast CuZnSOD (PDB code 1JCW) was used as the starting model for phase determination (*26*). Model adjustment was undertaken using all data (no σ cutoff) during multiple rounds of crystallographic refinement in X-PLOR (*43*) for the 15 atm of oxygen and H48C crystal systems and in SHELXL-93 (*44*) for the azide-bound system. A

Table 2: Crystallographic Data and Refinement for the Three Yeast CuZnSOD Molecules of This Paper[a,i]

	azide-bound[b]	H48C[c]	15 atm of oxygen[c]
unit cell dimensions (Å)	$a = b = 119.4$, $c = 74.5$	$a = b = 118.6$, $c = 75.4$	$a = b = 118.9$, $c = 75.2$
temperature (°C)	20	20	20
wavelength (Å)	1.54	1.54	1.07
crystal-to-plate distance (mm)	90	90	120
oscillation range (deg)	1.5	1.5	2.0
no. of observations	133918	46156	64930
no. of unique reflections	22142	17197	16754
no. of rounds[d]	8	6	5
completeness (%)[e]	98.5 (89.7)[f]	90.7 (75.8)[f]	87.7 (90.5)[f]
resolution range (Å)	90.0−1.70	50.0−1.80	50.0−1.80
R_{sym} (on I) (%)[g]	9.7 (42.1)[f]	8.0 (21.9)[f]	4.8 (14.8)[f]
R (%)	17.3	20.9	20.0
R_{free} (%)	20.8	25.8	25.4
$F/\sigma F$	>0	>0	>0
no. of protein atoms (not hydrogen)	1106	1102	1106
no. of metal ions	2	3[h]	2
no. of solvent atoms	145	117	116
rmsd from ideal values			
bond lengths (Å)	0.020	0.010	0.010
bond angles (deg)	2.5	1.5	1.5
dihedral angles (deg)	27.5	26.9	26.8
improper angles (deg)	2.9	1.3	1.4

[a] Refined models and their corresponding structure factors have been deposited in the Protein Data Bank. [b] Structure refined with SHELXL-93 (*44*). [c] Structure refined with X-PLOR 3.1 (*43*). [d] See text for definition. [e] Of all reflections to the high-resolution limit. [f] These numbers denote completeness in the highest resolution shells (azide-bound, 1.76−1.70 Å; H48C, 1.86−1.80 Å; 15 atm of oxygen, 1.86−1.80 Å). [g] R_{sym} = conventional discrepancy R-factor for scaling symmetry-related intensities. [h] Chloride has been modeled as an equatorial ligand. [i] Three-dimensional diffraction data were collected using a Rigaku RAXIS IV imaging plate detector (azide-bound and H48C) and a Mar 18 centimeter imaging plate at SSRL beamline 7−1 (15 atm of oxygen). The X-ray source for RAXIS data collection was a Rigaku RU-200 generator with focusing mirrors running at 50 kV, 100 mA. The data were reduced using the program DENZO (*63*).

"round" of refinement is defined as computational (least squares and/or molecular dynamics) refinement of the structure followed by visual inspection of electron density maps coupled with manual model rebuilding (when necessary), using the molecular graphics FRODO (*45*). No stereochemical constraints were imposed on the coordination geometries of the copper and zinc ions during refinement. Model atom positions were verified by the examination of conventional and simulated annealing omit maps (*46*). A total of 116, 145, and 117 water molecules were incorporated into the 15 atm of oxygen, azide-bound, and H48C models, respectively.

Comparison of Structures. Structural alignment of backbone atoms in all structures analyzed was accomplished using a modified version of the program ALIGN (*47*). H48C was arbitrarily chosen as the reference structure, and all other protein backbones were aligned to it [PDB codes 1JCW (*26*), 1SXC (*29*), 1XSO (*48*), 1SXZ (*49*), and 1AZV (*50*)]. Rotation and translation vectors resulting from these structural alignments were subsequently applied to the water molecules in each respective structure so they too could be compared. Simulated annealing omit maps (*46*) around metal atoms were calculated by omitting a 6 Å radius sphere around both the copper and zinc atoms and heating to 2500 K during the simulated-annealing protocol. Figures were created with the molecular graphics program SETOR (*51*). Atomic coordinates and diffraction data have been deposited in the Brookhaven Protein Data Bank with codes 2jcw (rljcwsf), 1b4l (r1b4lsf), 1yaz (rlyazsf), and 1b4t (r1b4tsf), for wild-type, 15 atm of oxygen, azide-bound, and H48C mutant structures, respectively.

Hazardous Procedures. Protective eyewear should be worn during pressurization of the capillary when using the modified goniometer head apparatus (*41*). In our experiments the capillaries reliably withstood up to 15 atm of pressure.

RESULTS

The three new yeast SOD structures are isomorphous with the previously reported wild type (*26*). Except for the critical details of atom positions in the copper binding sites and in some flexible solvent-exposed side chains, the structures are similar. Yeast wild-type, 15 atm of oxygen, and azide-bound backbone atoms superimpose onto the yeast H48C backbone with rms deviations of 0.16, 0.17, and 0.19 Å, respectively, for all main chain atoms. In addition, most bound water molecule positions in the active site channel region are conserved. Table 2 summarizes the X-ray data collection, processing, and refinement statistics for the 15 atm of oxygen, azide-bound, and H48C yeast CuZnSOD structures.

The refinement of 15 atm of oxygen yeast SOD can be summarized as follows: The final model contains 1106 protein atoms and 116 water molecules. The R-value is 20.0% (R_{free} = 25.4%; 10−1.8 Å, $\sigma > 0$). rms deviations from ideality for bond lengths and angles are 0.010 Å and 1.5°, respectively. The copper coordination geometry of 15 atm of oxygen yeast SOD is best described as trigonal planar, with His46, His48, and His120 acting as ligands. Figure 2 shows this copper binding site superimposed on electron density of the form $(2F_o - F_c)\alpha_c$ and $(F_o - F_c)\alpha_c$ from the same viewpoint as in Figure 1. The difference electron density shows elongation in the direction of copper displacement, perpendicular to the trigonal plane, with $>3\sigma$ peaks above and below the refined copper position.

The refinement of azide-bound yeast SOD can be summarized as follows: The final model contains 1106 protein atoms, 145 water molecules, and 1 azide anion. The R-value

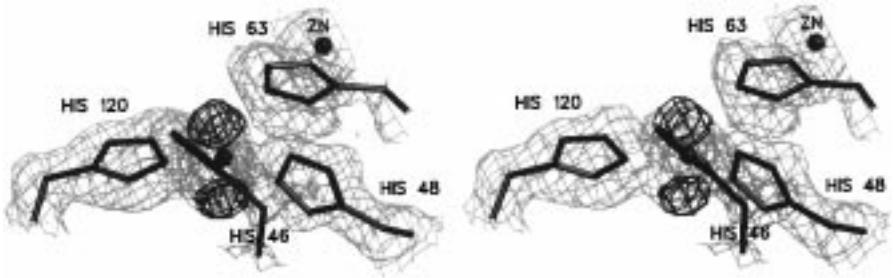

FIGURE 2: Atomic model for the active site atoms of 15 atm of oxygen yeast CuZnSOD superimposed on 1.8 Å resolution electron density of the form $(2F_o - F_c)\alpha_c$ contoured at 1σ (light cages) and of the form $(F_o - F_c)\alpha_c$ contoured at 3σ (dark cages) in the same orientation as in Figure 1. The copper ion has moved 0.37 Å approximately perpendicular to the trigonal plane relative to the wild-type Cu(I)ZnSOD copper position and shows two-state character suggestive of a mixture of oxidation states and binding geometries.

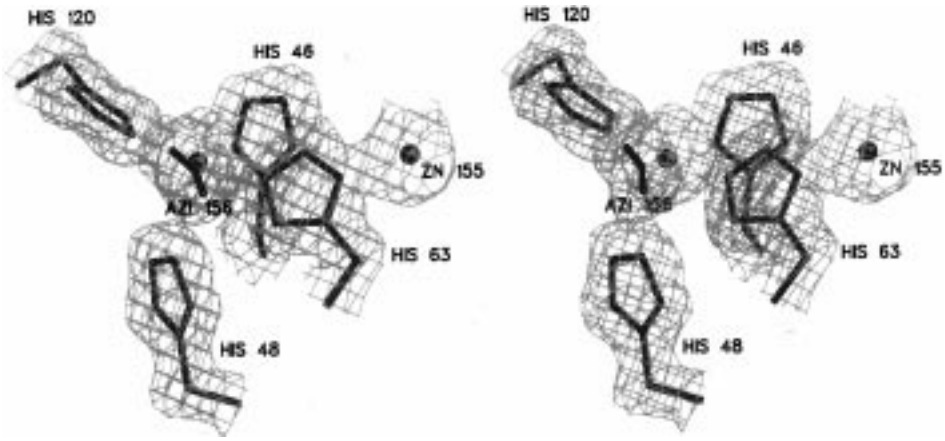

FIGURE 3: Atomic model for the active site atoms of azide-bound yeast CuZnSOD superimposed on 1.7 Å resolution electron density of the form $(2F_o - F_c)\alpha_c$ contoured at 1σ. The view is rotated approximately 80° in the vertical and 60° in the horizontal relative to Figures 1 and 2. Azide binds in an equatorial liganding position with His46, His63, and His120. His48 becomes an axial ligand with an increased bond length of 2.76 Å.

is 17.3% (R_{free} = 20.8%; 90−1.7 Å, $\sigma > 0$). rms deviations from ideality for bond lengths and angles are 0.020 Å and 2.5°, respectively. The azide-bound copper coordination geometry can best be described as square pyramidal, with His46, His63, His120, and azide making up the square plane, while His48 becomes the axial ligand upon azide binding. Figure 3 shows the refined model of this copper site superimposed on 1.7 Å resolution electron density of the form $(2F_o - F_c)\alpha_c$.

The refinement of the H48C yeast SOD can be summarized as follows: The final model contains 1102 protein atoms, 117 water molecules, and 1 chloride ion. The *R*-value is 20.9% (R_{free} = 25.8%; 10−1.8 Å, $\sigma > 0$). rms deviations from ideality for bond lengths and angles are 0.010 Å and 1.5°, respectively. The H48C yeast SOD copper coordination geometry is also square pyramidal, with His46, His63, His120, and chloride making up the square plane and H_2O acting as the axial ligand. Figure 4 shows the refined model of this copper binding site superimposed on 1.8 Å electron density. The view is as in Figure 3. Stereochemical properties of the three new structures compared to other selected CuZnSODs refined to a resolution greater than 2.0 Å are shown in Table 1 in the Supporting Information.

CuZnSOD subunits bREDa, bREDb, bABa, bABb, Xenoa, and Xenob superimpose onto yeast H48C with rms deviations of 0.51, 0.46, 0.49, 0.51, 0.48, and 0.53 Å, respectively, for main chain atoms. Rotation and translation vectors resulting from these alignments were applied to water molecules in the respective structures so they could be directly compared. Eleven water molecules present in the active site channel in the yeast wild-type structure were used as a reference (Table 2 in the Supporting Information). Their positions are shown in Figure 7. Except for three water molecules that are lost in the yeast and bovine azide-bound structures, the reference water molecules are almost completely conserved in the bovine reduced and *Xenopus laevis* CuZnSOD structures.

DISCUSSION

Influence of the SOD Rack and Crystal Contacts on the Copper Redox State. In this section, we draw on the numerous crystallographic (Table 1) and solution studies of CuZnSODs in addition to the three new structures reported here to propose a structure-based mechanism for SOD. We start by briefly reviewing literature studies that have described structural states of the copper environment in SODs. We go on to describe the additional states observed in the 15 atm of oxygen, azide-bound, and H48C structures reported here. In the final part of this section we describe a mechanism that encompasses these various states.

When taken together, the different yeast and bovine wild-type CuZnSOD crystal structures imply that a delicate balance exists between the free energies of the reduced and oxidized forms of the enzyme under physiological conditions. The crystal structure of wild-type yeast CuZnSOD, first determined to 2.5 Å resolution in space group $P2_12_12$ with two dimers per asymmetric unit (*19*) (PDB code 1SDY), has Cu(II) bound to four histidyl ligands in a coordination

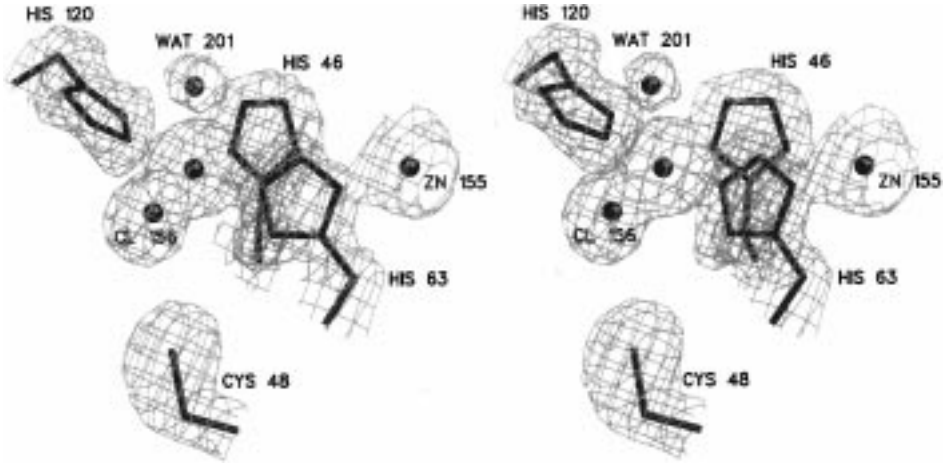

FIGURE 4: Atomic model for the copper binding site of the H48C mutant yeast CuZnSOD superimposed on 1.8 Å resolution electron density of the form $(2F_o - F_c)\alpha_c$ contoured at 1σ. The view is the same as in Figure 3. The newly introduced Cys48 does not coordinate the copper ion. Instead, a chloride ion binds equatorially in the square plane with His46, His63, and His120. The axial liganding position is filled by a water molecule (201). The position of this axial ligand is on the opposite side of the square plane when compared to the axial ligand in the azide-bound structure (Figure 3).

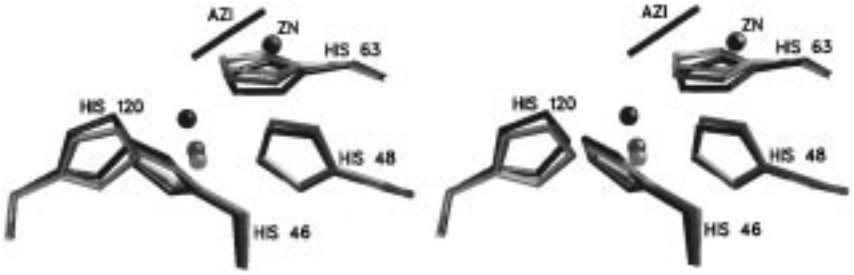

FIGURE 5: Effect of oxidation state of the copper ion on the geometry of the active site. Wild-type (light shading), 15 atm of oxygen (medium shading), and azide-bound (dark shading) yeast CuZnSOD active sites are superimposed on each other as described in Materials and Methods in approximately the same orientation as in Figures 1 and 2. As the oxidation state of copper increases, the copper ion moves perpendicularly to the trigonal plane formed by His46, His48, and His120 and toward the NE2 atom of the bridging imidazolate, His63.

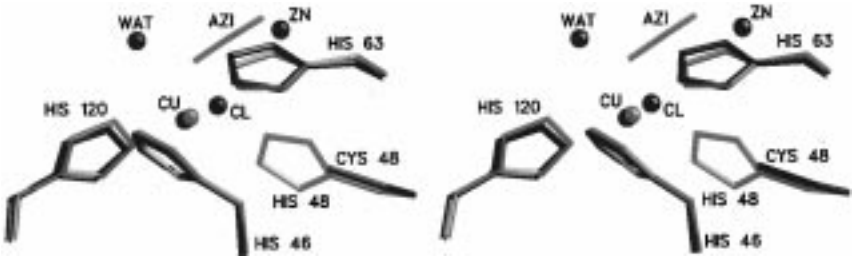

FIGURE 6: Effect of different copper ligands on the geometry of the CuZnSOD active site. Azide-bound (light shading) and H48C mutant (dark shading) yeast CuZnSOD copper binding sites are superimposed as described in Materials and Methods. The view is as in Figures 1, 2, and 6. The copper ions are in approximately the same position, with an intact imidazolate bridge, but the axial ligand identity and position are different (His48 in the azide-bound case and water in the H48C case). Notice that the square plane defined by His46, His63, His120, and azide is tilted approximately 40° relative to the square plane defined by His46, His63, His120, and chloride.

geometry described as an uneven distortion from a square plane. The imidazolate bridge, His63, links the copper and zinc ions in the four subunits (*19*). In contrast, the *R*32 wild-type yeast Cu(I)ZnSOD crystal structure exhibits a trigonal planar Cu(I) coordination and a broken imidazolate bridge with His63 detached from the copper (*26*). The influence of different crystal lattice contacts on the redox equilibrium suggests that subtle alterations in protein interactions are able to modulate bound metal ion redox potentials (*26, 50*). Because the energy changes in crystal contacts are believed to be of the order of ~1−5 kcal/mol, this suggests that the reduced and oxidized states of yeast SOD are within this range in these crystals (*52*).

In contrast to the yeast SOD structures, in which both intact and broken imidazolate bridge motifs are observed (*19, 26*), two bovine Cu(I) and Cu(II) structure determinations in space group $P2_12_12_1$ at pH 7.5 demonstrate an intact imidazolate bridge (PDB codes 1COB and 1SXC) (*27, 29, 53*). Although the Cu(II) ion was forcefully reduced using exogenous reductants, the coordination of the Cu(I) ion in the catalytic site was found to be unchanged from that of the Cu(II) form (*29*). This finding is contrary to results obtained from spectroscopic studies on the reduced enzyme in solution, which indicate that the imidazolate bridge between the Cu and Zn ions breaks upon copper reduction (*15, 22, 54, 55*). Although continuous electron density exists between the bovine Cu(I) ion and the imidazolate bridge in that structure, large anisotropic vibrations are present in subunit B, as evidenced by difference density peaks ($F_o - F_c$) positioned above (toward the NE2 atom of the bridging

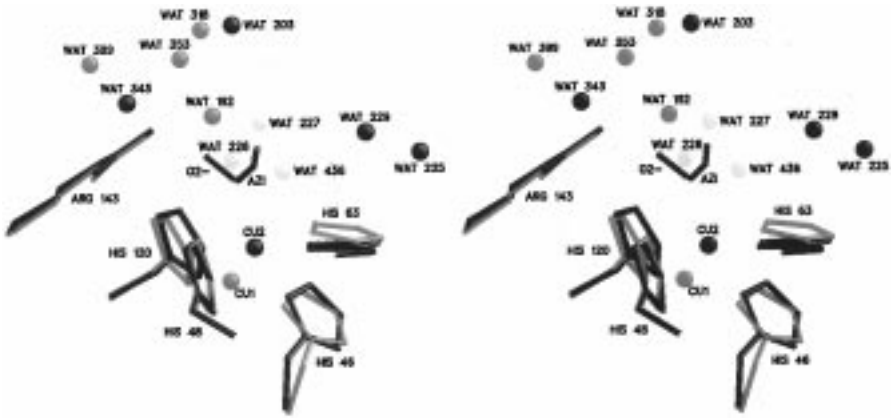

FIGURE 7: Wild-type (light shading) and azide-bound (dark shading) yeast CuZnSOD copper binding sites with conserved bound water molecules and a hypothetical site for a docked superoxide (dark shading). The water molecules shown are listed with the yeast wild-type numbering. Putative anion binding sites and a possible catalytic mechanism are described (see text). Water molecules which are invariant, nearly invariant, and displaced upon azide binding in the CuZnSOD structures are shown as dark, medium, and light spheres, respectively.

imidazolate) and below (toward the trigonal plane described previously) the copper. The largest anisotropic density peak corresponds to a copper position similar to that observed in the *R*32 yeast CuZnSOD structure; that is, a roughly trigonal planar geometry with three histidine ligands and a longer copper-to-His63 NE2 distance (*26, 29*).

A recent crystallographic determination of sodium dithionite-reduced bovine CuZnSOD in space group $C222_1$ at pH 5.0 also demonstrates an intact imidazolate bridge (PDB code 1SXN) (*56*). In this space group, one CuZnSOD monomer (subunit B) has many fewer crystal contacts than the other, resulting in average thermal parameters approximately 2-fold larger than the other monomer (subunit A). Although the electron density between the imidazolate bridge and the copper ion is continuous in both subunits, the electron density for the bridging imidazolate in subunit B shows evidence of some disorder. The authors suggest that this disorder implies a partial detachment from the copper ion, and they believe that the imidazolate bridge-intact conformation is favored by tighter crystal contacts while the imidazolate bridge-broken conformation is favored by a more "solution-like" environment (*56*). However, our experimental data on the imidazolate bridge-broken subunit of human FALS mutant G37R CuZnSOD and on the *R*32 yeast wild-type CuZnSOD (both are highly constrained in the crystal lattice) suggest the opposite trend (see below).

Human G37R CuZnSOD. Additional support for the existence of a balance between the redox forms of the enzyme and that protein−protein contacts play a role in this balance comes from the 1.9 Å resolution crystal structure of human FALS mutant G37R CuZnSOD (*50*). The Gly to Arg mutation is surface exposed and remote (∼18 Å) from the copper in the active site of the protein, which remains fully active (*57*). The hG37R structure displays the unique property of having the copper ion in one subunit of the dimer in an imidazolate bridge-intact, four-coordinate, Cu(II)-like liganding arrangement, while the other shows an imidazolate bridge-broken, three-coordinate, Cu(I)-like liganding arrangement. Despite the differences at the active site, the two subunits, which have distinct environments in the crystal ($P4_1$, one dimer in the asymmetric unit), superimpose with a rms deviation of only 0.21 Å. In contrast to the pH 5.0 bovine case described above, however, the imidazolate bridge-intact subunit has fewer crystal contacts and higher thermal parameters than the imidazolate bridge-broken subunit (*50, 56*).

In short, analysis of the yeast and bovine wild-type and human FALS G37R mutant crystal structures suggests that the nature of the protein−protein contacts in the crystal can influence the coordination geometry of the active site copper. In the yeast case, different crystal contacts in different space groups result in both reduced and oxidized copper in the absence of exogenous reductant (*19, 26*). In the pH 7.5 bovine case, identical protein−protein contacts in the oxidized and reduced $P2_12_12_1$ crystals predispose the copper to be in the imidazolate bridge-intact Cu(II) form, even in the presence of exogenous reductant (*29, 53*). In the pH 5.0 bovine $C222_1$ case, the more solution-like subunit displays a partially detached imidazolate bridge (*56*), while in the human FALS mutant G37R case, the more solution-like subunit displays an intact imidazolate bridge (*50*). Therefore, while it seems clear that the crystal contacts can influence copper coordination geometry, it is difficult to formulate general rules that would allow the prediction of this geometry based on number of crystal contacts or the relative "solution state" of a given CuZnSOD subunit.

15 Atm of Oxygen Yeast CuZnSOD. To explore further the balance between the oxidized and reduced forms of CuZnSOD and to examine the role of crystal contacts in this balance, we partially oxidized the copper ion in a colorless yeast wild-type Cu(I) *R*32 crystal by exposing it to ∼15 atm of oxygen prior to and during X-ray data collection. The oxygen treatment causes the crystals to turn light blue, indicative of some Cu(II) character. The refined structure of the active site looks generally similar to that of the *R*32 wild-type copper binding site, but there are some significant deviations. The copper ion is in a trigonal planar arrangement of His46, His48, and His120 ligands at distances of 2.06, 2.24, and 2.00 Å, respectively, and as in the Cu(I) *R*32 wild type, no electron density is observed between the copper ion and the NE2 atom of His63, which are 2.73 Å apart (3.16 Å in wild type).

The feature of SOD electron density we term copper elongation is evident in Figure 2, which shows the 15 atm of oxygen yeast CuZnSOD active site superimposed on 1.8 Å electron density of the form $(2F_o - F_c)\alpha_c$ and $(F_o - F_c)\alpha_c$ contoured at 1σ and 3σ, respectively. The view is identical to that in Figure 1. The oxygen treatment results in the

displacement of the copper ion 0.37 Å from its position in the wild-type structure toward the NE2 atom of the His63. Concomitant with this displacement, the copper−His48 distance increases from 2.06 Å in the wild-type structure to 2.24 Å in the 15 atm of oxygen structure. The elongated electron density (±∼1.2 Å from the refined copper ion center) of the copper ion is observed in a direction roughly perpendicular to the trigonal plane. We interpret this elongation as an increase in the ratio of oxidized:reduced copper coordination geometries in the refined model relative to the *R*32 wild type. That is, the copper elongation results from a mixture of two states of molecules in the imidazolate bridge-broken and bridge-intact conformations (see azide-bound bridge-intact conformation below). This mixture is approximately 50:50 as evidenced by the magnitude of the difference density peaks shown in Figure 2. This copper elongation is similar to that observed in the bovine reduced subunit B active site, even though it possesses an intact imidazolate bridge (*29*).

Azide-Bound Yeast CuZnSOD. The question of whether the superoxide substrate enters the first coordination sphere of either the Cu(II) or Cu(I) ions has not been fully resolved. In the case of Cu(II)ZnSOD, however, anions such as azide, cyanide, and fluoride bind directly to the Cu(II) ion (*10, 34, 35, 58*). It is likely, therefore, that superoxide enters into the first coordination sphere of the Cu(II) ion, forming a Cu(II)(O_2^-) complex, prior to the electron transfer that forms the products Cu(I) and O_2 (*33, 59*).

To complete the spectrum of copper redox states and coordination geometries in the *R*32 yeast CuZnSOD crystal system, we determined the structure of azide-bound CuZnSOD. Azide-bound crystals appeared yellow-green due to the azide−copper charge-transfer band at ∼375 nm. Figure 3 shows the yeast azide-bound copper site superimposed on 1.7 Å electron density of the form $(2F_o - F_c)\alpha_c$ contoured at 1σ. The azide-bound copper coordination geometry is imidazolate bridge-intact, square pyramidal with His46, His63, His120, and azide acting as equatorial ligands. The Cu−His46, Cu−His63, Cu−His120, and Cu−azide ligands are at distances of 2.05, 2.04, 2.11, and 2.15 Å, respectively. The copper ion moves 1.28 Å from its position in the Cu(I) wild-type structure, toward re-forming the imidazolate bridge with azide bound. The 1.28 Å displacement of the copper ion upon azide binding is followed by a concerted shift of the His120 NE2 atom of 0.52 Å, keeping its coordination distance to Cu(II) constant. His46, however, maintains its distance from the copper in both structures without movement.

As suggested in spectroscopic studies (*25, 60*) and later observed in the bovine azide-bound X-ray crystal structure (*49*), His48 becomes loosely associated with the copper ion upon azide binding. In the yeast azide-bound structure, His48 occupies an axial liganding position with its NE2 atom 2.76 Å from the copper (2.06, 2.24, and 2.65/2.75 Å in yeast wild-type, in yeast 15 atm of oxygen, and in the 2.1 Å bovine azide-bound structures, respectively). In contrast to the bovine azide-bound structure, however, the copper−distal nitrogen atom of azide is considerably closer to the guanidinium nitrogen of Arg143, at a distance of 3.25 Å (3.61/3.67 Å in bovine) (*49*). In the yeast azide-bound structure, the copper−distal azide nitrogen atom is on the midpoint of a line between the guanidinium nitrogen of Arg143 and an invariant ordered water molecule (229 in Figure 7). This midpoint position could correspond the so-called "anion binding site" previously observed in NMR studies (*36, 37*) (see below).

A recent study investigating the interaction of azide with oxidized and reduced bovine SOD using Fourier transform infrared spectroscopy (FTIR) suggests that azide does not directly coordinate to Cu(I) but instead remains in the active site pocket in electrostatic interaction with the guanidinium group of Arg141 (Arg143 in human and yeast) (*61*). In the Cu(I) form of the enzyme, azide could sit in the anion binding site mentioned above, equidistant between the hydrogen bond donors Arg143 NH2 and water 229 (Figure 7 and see below). Azide could potentially be in the same place in both the Cu(I) and Cu(II) forms of the enzyme, coordinating directly to the copper in the oxidized form at a distance of 2.15 Å but interacting weakly at a distance of ∼3.1 Å from the copper in the reduced form, due to copper movement toward the trigonal plane (Figure 7). The FTIR results at first seem in contradiction to the fact that we derive an azide-bound Cu(II) structure from a Cu(I) bridge-broken structure upon soaking in high concentrations of NaN_3. It is clear from examination of the yeast azide-bound model, however, that Cu(I) has been oxidized to Cu(II) presumably by O_2 in air. This oxidation occurs fairly rapidly and is additional evidence for the fine balance of redox states for CuZnSODs mentioned previously. Once the Cu(I) loses its electron, azide can form a strong bond with the Cu(II) with its concomitant movement into an imidazolate bridge-intact binding geometry.

Redox Cycle and Copper Movement. Together, the yeast wild-type, 15 atm of oxygen, and azide-bound structures illustrate a spectrum of copper positions and ligand geometries that presumably occur during the superoxide disproportionation mechanism in reaction 2 above. Figure 5 illustrates a superposition of all three structures, summarizing this movement. The copper ion is in a three-coordinate, bridge-broken conformation at a distance of 3.16 Å from the NE2 atom of His63 in the wild-type structure. Upon exposure to ∼15 atm of dioxygen, the copper moves 0.37 Å toward His63, resulting in a shortening of the Cu−His63 NE2 distance to 2.73 Å. Simultaneously, the Cu−His48 distance increases from 2.06 to 2.24 Å, and the NE2 atom of His63 moves toward the pseudotrigonal plane 0.28 Å from its wild-type position. From this conformation to the oxidized azide-bound structure, the copper moves an additional 0.92 Å to re-form the His63 imidazolate bridge with a bond distance of 2.04 Å, with concomitant lengthening of the Cu−His48 distance by an additional 0.52 Å. The NE2 atom of His63 moves another 0.38 Å toward the pseudotrigonal plane upon imidazolate bridge re-formation. The copper movement is tracked by His120, which maintains its 2.10 Å bond distance in all three structures. Presumably, the reverse movements occur during reaction 1 above. It should be noted that the His63 ring tilts dramatically on going from the reduced to the oxidized conformation, with the His63 NE2 atom moving a total of 0.66 Å in the process. This His63 ring tilt movement would be expected due to steric considerations if the NE2 atom becomes protonated/deprotonated during the cyclic reaction mechanism shown in reactions 1 and 2.

H48C Yeast CuZnSOD. The His48 ligand undergoes a conversion from a tightly associated equatorial ligand in the

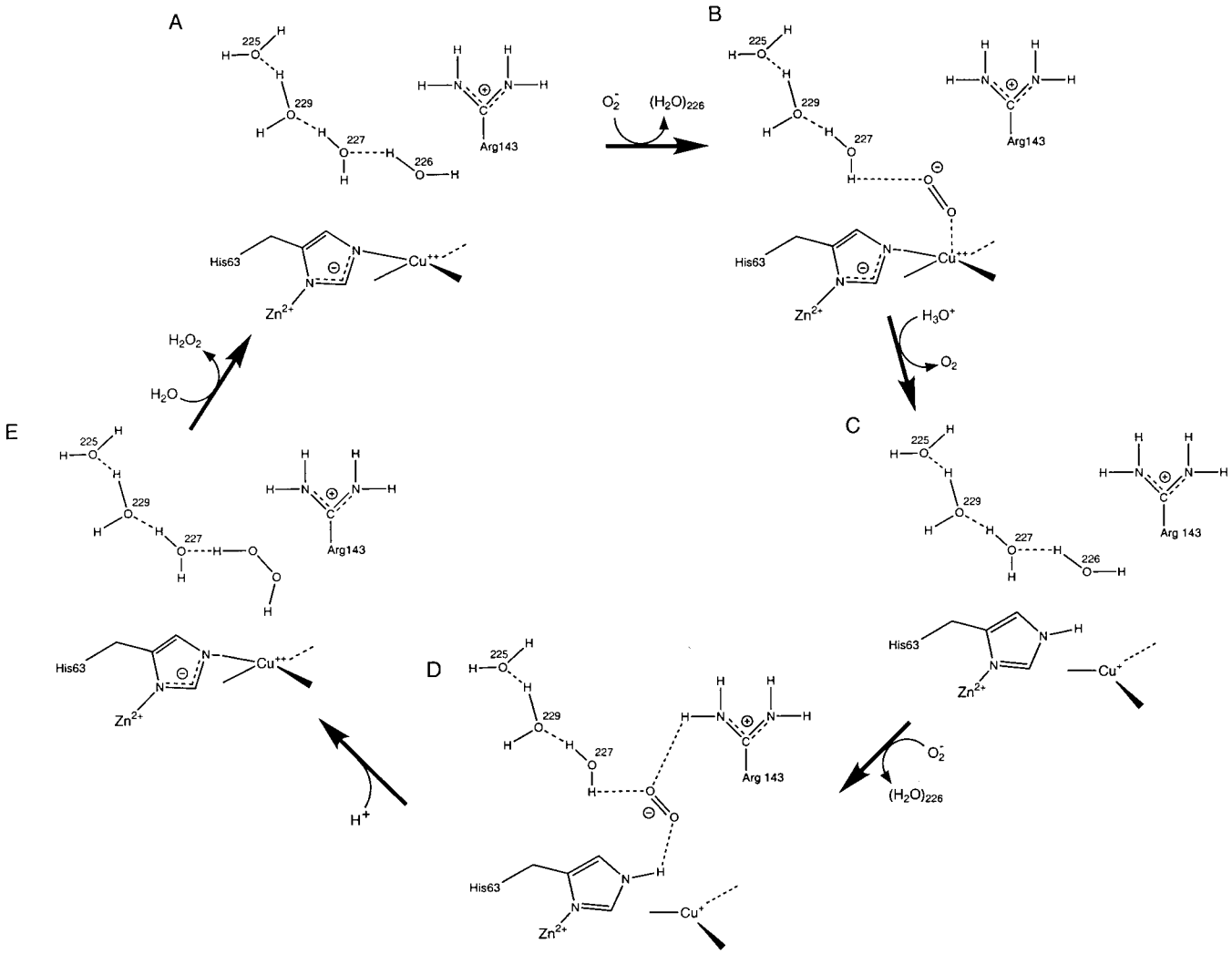

FIGURE 8: Schematic diagram of the catalytic cycle for CuZnSOD derived from Figure 7 (see text). (A) SOD Cu(II) resting state. Copper is in a distorted square planar conformation characteristic of Cu(II). (B) SOD inner sphere electron-transfer state. Superoxide enters the active site cavity, displaces Wat226, and binds directly to the copper ion and gives up its electron. (C) Cu(I) resting state. The histidine bridge breaks, oxygen diffuses out of the active site channel, and Wat226 enters. The NE2 atom of His63 may get its proton from bulk solvent. The copper is in a trigonal planar conformation characteristic of Cu(I). (D) SOD outer sphere electron-transfer state. Superoxide enters the active site cavity, displaces Wat226, and hydrogen bonds with Wat227 and the protonated NE2 atom of His63. (E) Completion of the cycle. Superoxide can accept an electron from copper and protons from Wat227 and His63 to form hydrogen peroxide. Peroxide diffuses out of the active site and is replaced by Wat226. The imidazolate bridge re-forms as copper becomes square planar. Waters 227, 229, and 225 form a hydrogen-bonded chain that is postulated to act as a proton shuttle in this step of the mechanism.

yeast wild-type structure (Cu−His48 NE2 distance = 2.06 Å) to a weakly associated axial ligand upon azide binding (Cu−His48 NE2 distance = 2.76 Å). To probe the importance of this residue as a determinant in copper binding, we converted it to cysteine via site-directed mutagenesis. First, we wanted to determine if the H48C mutant might bind copper in a "blue" or "type I" fashion with His46, His120, and Cys48 forming a trigonal planar liganding arrangement reminiscent of plastocyanin, azurin, and other cupredoxins. Second, in the event the H48C variant did not form a type I site, we were curious to see how the protein backbone, what we call the "SOD rack", would influence copper binding in this nonnative site. Figure 4 shows the refined H48C copper binding site superimposed on 1.8 Å electron density of the form $(2F_o - F_c)\alpha_c$ contoured at 1σ. The potential cysteinate ligand is seemingly ignored by the copper ion. The copper coordination is square pyramidal, with His46, His63, His120, and chloride acting as equatorial ligands at distances of 1.99, 2.09, 2.12, and 2.13 Å, respectively. The square plane in this copper coordination sphere is tilted relative to the square plane in the azide-bound yeast structure by ~40° (Figure 6). The H_2O axial ligand in H48C is on the opposite side of the square plane than the axial histidine ligand in the azide-inhibited structure.

In Figure 4, a chloride ion is modeled as an equatorial ligand because of the following: (a) Water built into this position returns positive difference density peaks, indicating that a more electron-dense species is required. Chloride returns no difference density peaks. (b) Chloride is present in the crystallization condition at a concentration of 50 mM. Although chloride ion has not been observed to bind directly to copper in the native enzyme (*33*), the loss of His48 causes the copper to reorganize its ligand field in the SOD rack and to acquire the new axial water ligand. This reorganization may allow chloride ion to bind equatorially since there is no His48−Cu interaction with which to compete.

Active Site Water Structure and Catalytic Mechanism. Ordered water molecules in and around the active site cavity

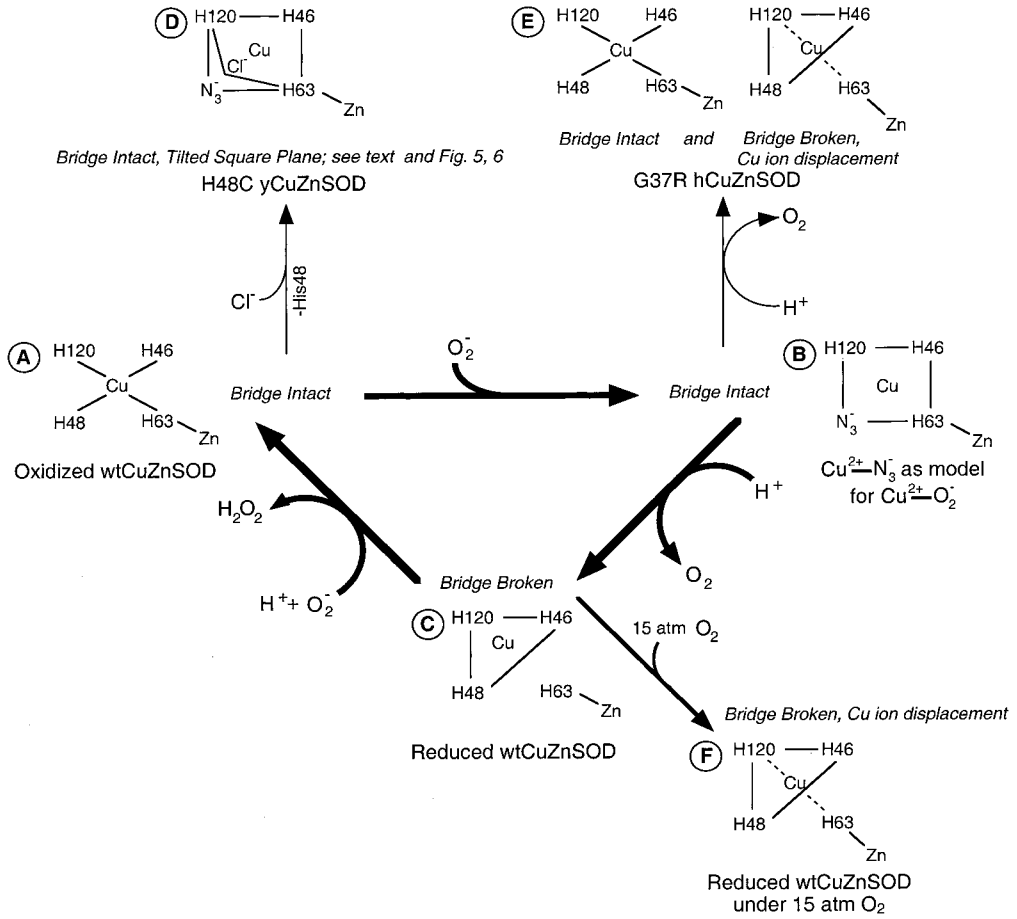

FIGURE 9: Summary of known crystal structures that correspond to various steps of the catalytic cycle in Figure 8. All ligands are shown with numbering based on the yeast and human enzymes. (A) Bridge-intact square planar Cu(II)ZnSODs (*8*, *18*, *20*, *48*, *53*, *64*, *65*) corresponding to panel A of Figure 8; (B) bridge-intact square pyramidal with ligand bound (yeast azide-bound in this study) (*21*, *49*) corresponding to panel B of Figure 8; (C) bridge-broken trigonal planar (*26*) corresponding to panel C of Figure 8; (D) bridge- intact square pyramidal with tilted square plane and novel chloride ligand (yeast H48C in this study) corresponding to no step of Figure 8 because H48C is off the cycle; (E) one bridge-intact and one bridge-broken subunit (*50*) corresponding to a combination of panels A and C of Figure 8; (F) bridge-broken with copper ion displacement (15 atm of oxygen pressure in this study). The dotted lines and the slight shift of Cu on panels E and F indicate a mixture of the two states represented by panels A and C of Figure 8.

are largely conserved in high-resolution CuZnSOD X-ray structures. Table 2 in the Supporting Information highlights 11 bound water molecules found in the yeast wild-type active site channel (*26*) and illustrates their presence or absence in yeast 15 atm of oxygen (1.8 Å, this study), yeast azide-bound (1.7 Å, this study), yeast H48C (1.8 Å, this study), bovine azide-bound (2.1 Å, PDB code 1SXZ, subunits A and B) (*49*), bovine reduced (1.9 Å, PDB code 1SXC, subunits A and B) (*29*), and *X. laevis* (1.5 Å, PDB code 1XSO, subunits A and B) (*48*). These CuZnSOD subunits with their respective water molecules were structurally aligned as described in Materials and Methods. Figure 7 shows a superposition of the yeast wild-type and azide-bound active site residues highlighting the positions of these 11 water molecules (yeast wild-type numbering) in the active site channel. Except for Wat226, Wat227, and Wat436, which are displaced upon azide binding in both the yeast and bovine structures, and Wat318, which is further out from the active site copper, most of the remaining water molecules are conserved in all structures. Superoxide anion is very strongly solvated by hydrogen-bonded water molecules in aqueous solution. These waters of solvation must either be dragged by superoxide into the active site channel or, more likely, be replaced by other hydrogen bond donors as superoxide travels toward the copper ion. The presence of strongly conserved water molecules in structurally characterized CuZnSOD from a wide variety of species is thus of particular importance in attempting to map the superoxide trajectory into and through the active site channel.

Figure 7 also illustrates the position of the putative anion binding site described previously. In the yeast azide-bound structure, the copper−distal nitrogen of azide sits on the midpoint of a line between the guanidinium nitrogen of Arg143 and Wat229 (3.2 Å away from both). Wat229 is invariant in all the structures and is anchored by two additional hydrogen bonds to the amide nitrogen of His63 and to the carbonyl oxygen of Lys136. In the absence of azide, Wat227 fills this midpoint position. Recent FTIR studies (*61*) on both the oxidized and reduced forms of CuZnSOD have shown that the antisymmetric stretching band of azide was observed to shift to higher energy upon coordination to Cu(II)ZnSOD, consistent with direct binding to the copper. In the Cu(I)ZnSOD case, however, the azide band was shifted to lower energy, similar to that observed upon reaction of azide with free arginine or lysine. These results were interpreted to mean that azide does not directly coordinate to copper in the reduced form of the enzyme but

instead remains associated with Arg143 in the active site channel.

It is likely that superoxide binds to CuZnSOD in a fashion similar to azide during the catalytic cycle. If this is the case, then superoxide binds directly to Cu(II) in reaction 1 (inner sphere electron transfer) but remains in the anion binding site and accepts in reaction 2 its electron when an oxygen atom is approximately 3 Å distant from the copper (outer sphere electron transfer) (*62*). To examine this possibility further, we modeled superoxide into the active site cavity. Figure 7 shows that the copper−proximal oxygen of superoxide (O_2^-) was placed in the same position as the copper−proximal nitrogen of azide, which is where it presumably sits in the inner sphere electron transfer of reaction 1. The copper−distal oxygen of superoxide was oriented such that it can hydrogen bond to the guanidinium nitrogen of Arg143 at a distance of 2.7 Å while simultaneously making a hydrogen bond to Wat227, also at a distance of 2.5 Å. The copper−proximal oxygen atom of superoxide is 2.8 Å from the (protonated) NE2 atom of His63. This orientation of superoxide is almost identical to that observed for cyanide in the 1.7 Å cyanide-bound *X. laevis* CuZnSOD structure (*21*). This model permits us to propose a structure-based cyclic mechanism for CuZnSOD action.

The catalytic cycle based on these aligned structures and our superoxide docking model can be summarized as follows (Figure 8): The reaction starts when superoxide is electrostatically guided into the active site channel (*31*, *32*). It then associates with Arg143 and displaces Wat226. Superoxide binds directly to Cu(II) and delivers its electron via an inner sphere mechanism. Dioxygen, no longer charged and electrostatically attracted to Arg143, diffuses out of the active site channel and is replaced by Wat226, which is hydrogen bonded to Wat227 at a distance of 2.7 Å. In the second half of the reaction cycle (Figures 7 and 8), superoxide is electrostatically drawn into the active site channel, displaces Wat226, and forms hydrogen bonds with Arg143 and Wat227. As the electron is accepted from the Cu(I) via an outer sphere electron-transfer mechanism, superoxide takes a proton simultaneously from Wat227 and the NE2 atom of the (tilted) bridging imidazolate, His63. The Cu(II) ion can now move to re-form the (deprotonated) histidine bridge. Electrically neutral hydrogen peroxide diffuses out of the active site channel and is replaced by Wat226. A chain of water molecules including Wat229 and Wat225 can relay protons to the active site, replenishing those delivered to form peroxide.

CONCLUSIONS

We determined three-dimensional structures of three new yeast CuZnSODs and compared them to other existing CuZnSOD structures. Yeast and bovine wild type and human G37R mutant structures suggest that weak protein−protein contacts in the crystal can influence the oxidation state of the active site copper. Significant protein backbone changes are not observed, and therefore do not appear to play a role in the catalytic cycle. On the basis of the FTIR studies (*61*), azide-bound structures, and our superoxide-docking model derived from multiple structure alignments of high-resolution CuZnSODs, superoxide probably enters the first coordination sphere of the copper ion during the Cu(II) portion of the catalytic cycle but not during the Cu(I) portion. In the Cu(I) portion, a proton from a highly conserved water molecule and from the NE2 atom of His63 could be donated to superoxide to form hydrogen peroxide. The 1.28 Å copper movement and tilt of His63 would facilitate this process. Figure 9 summarizes the structural states for the various steps of the superoxide disproportionation mechanism.

ACKNOWLEDGMENT

Discussions with D. Anderson, D. Cascio, T. J. Lyons, and J. J. Goto are gratefully acknowledged. We are indebted to Stephen Holloway and Sue Weintraub for aid in the creation of figures and to Michael Stowell and Mike Soltis for assistance in the collection of the 15 atm of oxygen data. We thank K. Djinovic-Carugo for the bovine azide-bound CuZnSOD coordinates.

SUPPORTING INFORMATION AVAILABLE

Table 1 showing stereochemical properties of the azide-bound, H48C, 15 atm of oxygen, and wild-type structures (these are compared to $subunit_{broken}$ of human FALS mutant G37R (*50*), subunit A of bovine reduced (*29*), and subunit A of *X. laevis* CuZnSOD (*48*), structures that have all been refined to finer than 2.0 Å resolution) and Table 2 summarizing the presence or absence of conserved bound water molecules in the immediate vicinity of the active site channel for the yeast 15 atm of oxygen, azide-bound, H84C, and wild-type structures (the comparison of water molecules was performed as described in Materials and Methods). This material is available free of charge via the Internet at http://pubs.acs.org.

REFERENCES

1. Davies, K. J. (1995) *Biochem. Soc. Symp. 61*, 1−31.
2. Richter, C., Gogvadze, V., Laffranchi, R., Schlapbach, R., Schweizer, M., Suter, M., Walter, P., and Yaffee, M. (1995) *Biochim. Biophys. Acta 1271*, 67−74.
3. Balentine, J. D. (1982) in *Pathology of Oxygen Toxicity*, p 359, Academic Press, New York.
4. Meier, B., Radeke, H. H., Selle, S., Younes, M., Sies, H., Resch, K., and Habermehl, G. G. (1989) *Biochem. J. 263*, 539−545.
5. Valentine, J. S., Wertz, D. L., Lyons, T. J., Liou, L. L., Goto, J. J., and Gralla, E. B. (1998) *Curr. Opin. Chem. Biol. 2*, 253−262.
6. Fridovich, I. (1989) *J. Biol. Chem. 264*, 7761−7764.
7. Valentine, J. S. (1998) in *Metal Ions in Biological Systems* (Sigel and Sigel, Eds.) Marcel Dekker, Inc., New York (in press).
8. Tainer, J. A., Getzoff, E. D., Beem, K. M., Richardson, J. S., and Richardson, D. C. (1982) *J. Mol. Biol. 160*, 181−217.
9. Rotilio, G., Morpurgo, L., Giovagnoli, C., Calabrese, L., and Mondovi, B. (1972) *Biochemistry 11*, 2187−2192.
10. Rotilio, G., Bray, R. C., and Fielden, E. M. (1972) *Biochim. Biophys. Acta 268*, 605−609.
11. Klug-Roth, D., Fridovich, I., and Rabini, J. (1973) *J. Am. Chem. Soc. 95*, 2786−2790.
12. Fielden, E. M., Roberts, P. B., Bray, R. C., Lowe, D. J., Mautner, G. N., Rotilio, G., and Calabrese, L. (1974) *Biochem. J. 139*, 49−60.
13. Valentine, J. S., and Pantoliano, M. W. (1981) in *Copper Proteins* (Spiro, T. G., Ed.) pp 292−358, John Wiley and Sons, Inc., New York.
14. Tainer, J. A., Getzoff, E. D., Richardson, J. S., and Richardson, D. C. (1983) *Nature 306*, 284−287.

15. Bertini, I., Luchinat, C., and Monnanni, R. (1985) *J. Am. Chem. Soc. 107*, 2178−2179.
16. Bertini, I., Banci, L., and Piccioli, M. (1990) *Coord. Chem. Rev. 100*, 67−103.
17. Bannister, J. V., Bannister, W. H., and Rotilio, G. (1987) *CRC Crit. Rev. Biochem. 22*, 111−180.
18. Kitagawa, Y., Tanaka, N., Hata, Y., Kusonoki, M., Lee, G. P., Katsube, Y., Asada, K., Aibara, S., and Morita, Y. J. (1991) *J. Biochem. (Tokyo) 109*, 477−485.
19. Djinovic, K., Gatti, G., Coda, A., Antolini, L., Pelosi, G., Desideri, A., Falconi, M., Marmocchi, F., Rotilio, G., and Bolognesi, M. (1992) *J. Mol. Biol. 225*, 791−809.
20. Parge, H. E., Hallewell, R. A., and Tainer, J. A. (1992) *Proc. Natl. Acad. Sci. U.S.A. 89*, 6109−6113.
21. Djinovic-Carugo, K., Battistoni, A., Carri, M. T., Polticelli, F., Desideri, A., Rotilio, G., Coda, A., and Bolognesi, M. (1994) *FEBS Lett. 349*, 93−98.
22. Blackburn, N. J., Hasnain, S. S., Binsted, N., Diakun, G. P., Garner, C. D., and Knowles, P. F. (1984) *Biochem. J. 219*, 985−990.
23. Terenzi, M., Rigo, A., Franconi, C., Mondovi, B., Calabrese, L., and Rotilio, G. (1974) *Biochim. Biophys. Acta 351*, 230−236.
24. Bertini, I., Banci, L., Brown, R. D., III, Koenig, S. H., and Luchinat, C. (1988) *Inorg. Chem. 27*, 951.
25. Banci, L., Bertini, I., Luchinat, C., and Scozzafava, A. (1989) *J. Biol. Chem. 264*, 9742−9744.
26. Ogihara, N. L., Parge, H. E., Hart, P. J., Weiss, M. S., Goto, J. J., Crane, B. R., Tsang, J., Slater, K., Roe, J. A., Valentine, J. S., Eisenberg, D., and Tainer, J. A. (1996) *Biochemistry 35*, 2316−2321.
27. Banci, L., Bertini, I., Bruni, B., Carloni, P., Luchinat, C., Mangani, S., Orioli, P. L., Piccioli, M., Rypneiwski, W. R., and Wilson, K. S. (1994) *Biochem. Biophys. Res. Commun. 202*, 1088−1095.
28. Murphy, L. M., Strange, R. W., and Hasnain, S. S. (1997) *Structure 5*, 371−379.
29. Rypniewski, W. R., Mangani, S., Bruni, B., Orioli, P. L., Casati, M., and Wilson, K. S. (1995) *J. Mol. Biol. 251*, 282−296.
30. Tainer, J. A., Hallewell, R. A., Roberts, V. R., Parge, H. E., and Getzoff, E. D. (1988) in *Oxygen Radicals in Biology and Medicine* (Simic, M. G., Taylor, K. A., Ward, J. F., and Sontag, C. V., Eds.) pp 635−640, Plenum Press, New York.
31. Getzoff, E. D., Tainer, J. A., Stempien, M. M., Bell, G. I., and Hallewell, R. A. (1989) *Proteins 5*, 322−336.
32. Getzoff, E. D., Cabelli, D. E., Fisher, C. L., Parge, H. E., Viezzoli, M. S., Banci, L., and Hallewell, R. A. (1992) *Nature 358*, 347−351.
33. Bertini, I., Mangani, S., and Viezzoli, M. S. (1998) in *Advances in Inorganic Chemistry*, pp 127−250, Academic Press, New York.
34. Rigo, A., Viglino, P., and Rotilio, G. (1975) *Biochem. Biophys. Res. Commun. 63*, 1013−1018.
35. Rigo, A., Stevanato, R., Viglino, P., and Rotilio, G. (1977) *Biochem. Biophys. Res. Commun. 79*, 776−783.
36. Mota de Freitas, D., Luchinat, C., Banci, L., Bertini, I., and Valentine, J. S. (1987) *Inorg. Chem. 26*, 2788−2791.
37. Mota de Freitas, D., Ming, L., Ramasamy, R., and Valentine, J. S. (1990) *Inorg. Chem. 29*, 3512−3518.
38. Lu, Y., LaCroix, L. B., Lowrey, M. D., Solomon, E. I., Bender, C. J., Peisach, J., Roe, J. A., Gralla, E. B., and Valentine, J. S. (1993) *J. Am. Chem. Soc. 115*, 5907−5918.
39. Lu, Y. (1992) Ph.D. Dissertation, UCLA, Los Angeles, CA.
40. Nishida, C. R., Gralla, E. B., and Valentine, J. S. (1994) *Proc. Natl. Acad. Sci. U.S.A. 91*, 9906−9910.
41. Stowell, M. H. B., Soltis, S. M., Kisker C., Peters, J. W., Schindelin, H., Cascio, D., Beamer, L., Hart, P. J., Eisenberg, D., Wiener, M., Whitby, F. G., and Rees, D. C. (1996) *J. Appl. Crystallogr. 29*, 608−613.
42. Anderson, D. H. (1986) Ph.D. Thesis, The University of California, San Diego.
43. Brünger, A. T. (1988) in *Crystallographic Computing 4: Techniques and New Technologies* (Issacs, N. W., and Taylor, M. R., Eds.) pp 126−140, Clarendon Press, Oxford.
44. Sheldrick, G. M., and Schneider, T. R. (1997) *Methods Enzymol. 277*, 319−343.
45. Jones, T. A. (1978) *J. Appl. Crystallogr. 11*, 268−272.
46. Hodel, A., Kim, S. H., and Brünger, A. T. (1992) *Acta Crystallogr. A48*, 851−858.
47. Satow, Y., Cohen, G. H., Padlan, E. A., and Davies, D. R. (1986) *J. Mol. Biol. 190*, 593−604.
48. Djinovic-Carugo, K., Battistoni, A., Carri, M., Polticelli, F., Desideri, A., Rotilio, G., Coda, A., Wilson, K., and Bolognesi, M. (1996) *Acta Crystallogr. D52*, 176.
49. Djinovic, K., Polticelli, F., Desideri, A., Rotilio, G., Wilson, K., and Bolognesi, M. (1994) *J. Mol. Biol. 240*, 179−183.
50. Hart, P. J., Liu, H., Pellegrini, M., Nersissian, A. M., Gralla, E. B., Valentine, J. S., and Eisenberg, D. (1998) *Protein Sci. 7*, 545−555.
51. Evans, S. V. (1993) *J. Mol. Graphics 11*, 134−138.
52. Perutz, M. F. (1965) *J. Mol. Biol. 13*, 646−668.
53. Djinovic, K., Coda, A., Antolini, L., Pelosi, G., Desideri, A., Falconi, M., Rotilio, G., and Bolognesi, M. (1992) *J. Mol. Biol. 226*, 227−238.
54. Moss, T. H., and Fee, J. A. (1975) *Biochem. Biophys. Res. Commun. 66*, 799−808.
55. Bailey, D. B., Ellis, P. D., and Fee, J. A. (1980) *Biochemistry 19*, 591−596.
56. Ferraroni, M., Rypniewski, W. R., Bruni, B., Orioli, P., and Mangani, S. (1998) *J. Biol. Inorg. Chem. 3*, 411−422.
57. Borchelt, D. R., Lee, M. K., Slunt, H. S., Guarnieri, M., Xu, Z. S., Wong, P. C., Brown, R. H., Price, D. L., Sisodia, S. S, and Cleveland, D. W. (1994) *Proc. Natl. Acad. Sci. U.S.A. 91*, 8292−8296.
58. Fee, J. A., and Gaber, B. P. (1972) *J. Biol. Chem. 247*, 60−65.
59. Cabelli, D. E., Allen, D., Bielski, B. H., and Holcman, J. (1989) *J. Biol. Chem. 264*, 9967−9971.
60. Banci, L., Bencini, A., Bertini, I., Luchinat, C., and Piccioli, M. (1990) *Inorg. Chem. 29*, 4867−4873.
61. Leone, M., Cupane, A., Militello, V., Stroppolo, M. E., and Desideri, A. (1998) *Biochemistry 37*, 4459−4464.
62. Cabelli, D., Riley, D., Rodriguez, J., Valentine, J. S., and Zhu, H. (1998) in *Biomimetic Oxidations Catalyzed by Transition Metal Complexes* (Meunier, B., Ed.) Imperial College Press, London (in press).
63. Otwinowski, Z. (1993) in *Proceedings of the CCP4 Study Weekend: Data Collection and Processing* (Sawyer, L., Issacs, N., and Bailey, S., Eds.) pp 56−62, SERC Laboratory, Daresbury, England.
64. Deng, H. X., Hentati, A., Tainer, J. A., Iqbal, Z., Cayabyab, A., Hung, W. Y., Getzoff, E. D., Hu, P., Herzfeldt, B., Roos, R. P., Warner, C., Deng, G., Soriano, E., Smyth, C., Parge, H. E., Ahmed, A., Roses, A. D., Hallewell, R. A., Pericak-Vance, M. A., and Siddique, T. (1993) *Science 261*, 1047−1051.
65. McRee, D. E., Redford, S. M., Getzoff, E. D., Lepock, J. R., Hallewell, R. A., and Tainer, J. A. (1990) *J. Biol. Chem. 265*, 14234−14241.

BI982284U